

# TROPICAL CYCLONE GENERATED ROGUE WAVES

Clarence O. Collins III

The Rosenstiel School for Marine and Atmospheric Science

4600 Rickenbacker Causeway, Miami, FL, USA, 33149

email: [tcollins@rsmas.miami.edu](mailto:tcollins@rsmas.miami.edu)

## 1. INTRODUCTION

This paper introduces a new deep sea dataset for the study of rogue and extreme rogue waves: the first is defined as a singular wave height greater than twice the significant wave height and the latter has the additional criteria of a wave height of 15 m or greater. This dataset is particularly unique due to the measurement of near field winds and waves from 4 major tropical cyclones and the swell from a 5<sup>th</sup>. The introductory subsections include a primer on rogue waves, an overview of the field campaign, and a review of tropical cyclone (TC) generated sea states in the context of this study. The subsections under methods delve into detail about the mooring characteristics, buoy design, data analysis, and treatment of errors. The results section explains the timing of storm passages and attempts to objectively define periods in the data when the sea state is dominated by (and lacks) TC activity. Then, some simple analysis is presented of the two periods (TC and non-TC) for (1) number of rogue waves observed and (2) spectral characteristics related to unstable seas. The paper concludes with a discussion of the results and the potential of future work with this data.

### 1.1 ROGUE WAVES

Mariners and sea goers have long described encountering a singular wave of staggering size, a wave at least twice the height of any other wave seen around that time. Traditionally, scientists have not paid much attention to these stories; unusually large waves were chalked up to sailing myth and lore. However, it is now known that rogue waves are real and pose a serious danger to human life. This presents the strongest motivation for the study of rogue waves, not to mention the countless damages caused to platforms, ships, and other structures around the world. (Dysthe, Krogstad, & Müller, 2008; Tamura, Waseda, & Miyazawa, 2009; Waseda, Tamura, & Kinoshita, 2012)

A rogue wave (also referred to as an extreme wave, freak wave, killer wave, three sisters, wall of water, hole in the sea, abnormal wave, etc.) is a wave which meets one of two common criteria. An apparent wave height (i.e. crest to trough),  $H$ , twice the significant wave height or a crest height,  $\eta_c$ , 1.25 times the significant wave height. The significant wave height, SWH, may be described as the average of the 1/3 highest waves (Dysthe, Krogstad, & Müller, 2008). The specifics of these metrics will be described in section 2.3.

This is a statistical definition, so rogue waves, although rare, are bound to appear given enough time (i.e. over the course of many, many wave periods). This leads to the question: given a certain number of waves (and stationary statistics) how many will be extreme waves? Given

linear, Gaussian waves, the probability of observing an extreme wave is about 1 in 3,000 waves and the probability is somewhat greater with second-order weakly non-linear wave theory (Waseda, Kinoshita, & Tamura, 2009).

It has been shown that 2<sup>nd</sup> order wave theory (Stokes expansion) can well explain the wave height statistics under most conditions, but there are circumstances in which the number of extreme waves observed is far greater than what one would expect. Why is this? What is the physical mechanism responsible and under what conditions is it likely to occur?

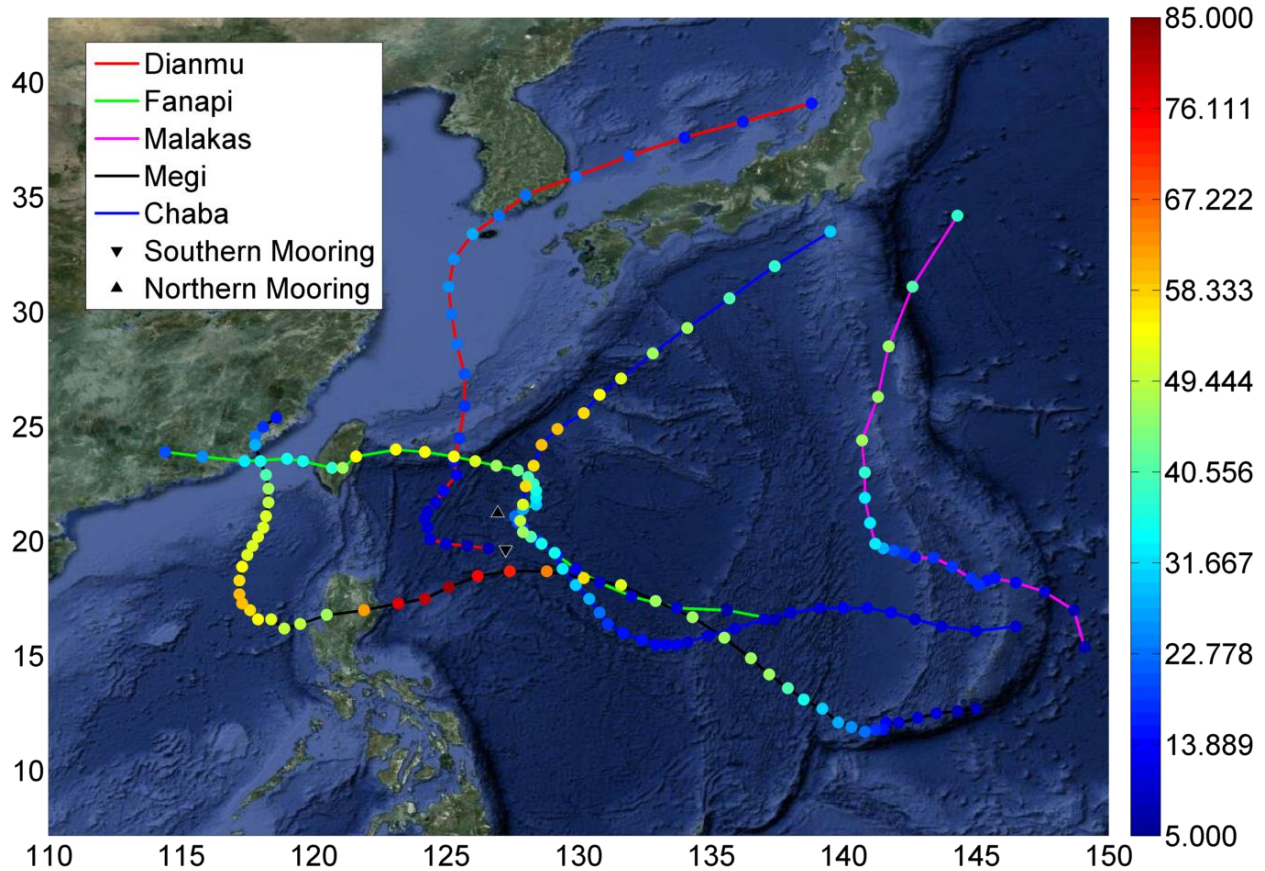


Figure 1) Map of the Philippine Sea. The northern mooring location is marked by the upward pointing black triangle and the southern mooring by the downward pointing black triangle. The best estimate storm tracks for Dianmu, Fanapi, Malakas, Megi, and Chaba are marked in solid red, green, magenta, black, and blue, respectively. The estimated maximum wind speed [ $\text{m s}^{-1}$ ] is denoted by the colored circles. The wind speed ranges from 5 to 85  $\text{m s}^{-1}$  (blue to red).

Large waves have been observed or reported in strong currents such as the Alguhas, the Gulf Stream, and the Kuroshio. Waves may be focused through refraction in strong currents (as well as varying bathymetry), but extreme waves observed in deep water outside the influence of strong currents require another explanation. Non-linear focusing of wave energy via modulation instability (i.e. Benjamin-Feir (B-F) type instability) is the likely culprit. This is a mechanism by which monochromatic wave trains are destabilized by small perturbations or disturbances. Under the right conditions, these initially small disturbances may grow at the expense of surrounding waves. This is an exciting and active area of research. Recent work has included careful laboratory measurements, spectral modeling, and numerical simulations (Tamura, Waseda, & Miyazawa, 2009; Waseda et al., 2011; Waseda, 1999).

The general consensus is that there are conditions which, in combination, are conducive to increasing the probability of observing an extreme wave (due to the B-F instability), for example: 1) when wave energy is concentrated in a narrow band of frequencies (i.e. very peaked spectra), 2) when waves are steep, and 3) when wave energy is concentrated in a narrow range of directions (i.e. spectra with low directional spread). The first two conditions may be combined into a parameter referred to as the B-F index (BFI) (Janssen, 2003). It is hypothesized that this consensus will hold for field observations, but there is a conspicuous dearth of field data. Field data is simply difficult to obtain, this is especially true for directional wave data (Waseda et al., 2011). This paper attempts to fill in a bit of this knowledge gap by exploiting high quality data from a recent ONR field experiment.

## 1.2 ITOP EXPERIMENT

In late 2010, the air-sea interaction research group at the University of Miami (UM) was involved in the international collaborative Office of Naval Research (ONR) sponsored field campaign called Impact of Typhoons on the Ocean in the Pacific (ITOP) 750 km off the eastern coast of Taiwan in the Philippine Sea. The UM group installed two moorings, and each mooring site included 2 buoys. One buoy with a 6 m Naval Oceanographic Meteorological Automatic Device (NOMAD) type hull dubbed the Extreme Air-Sea Interaction (EASI) buoy (Drennan et al. submitted to JTECH) was moored to the sea bed. The second buoy, an Air-Sea Interaction Spar (ASIS) buoy (Graber et al., 2000), was tethered to EASI by a 60 m braided steel line.

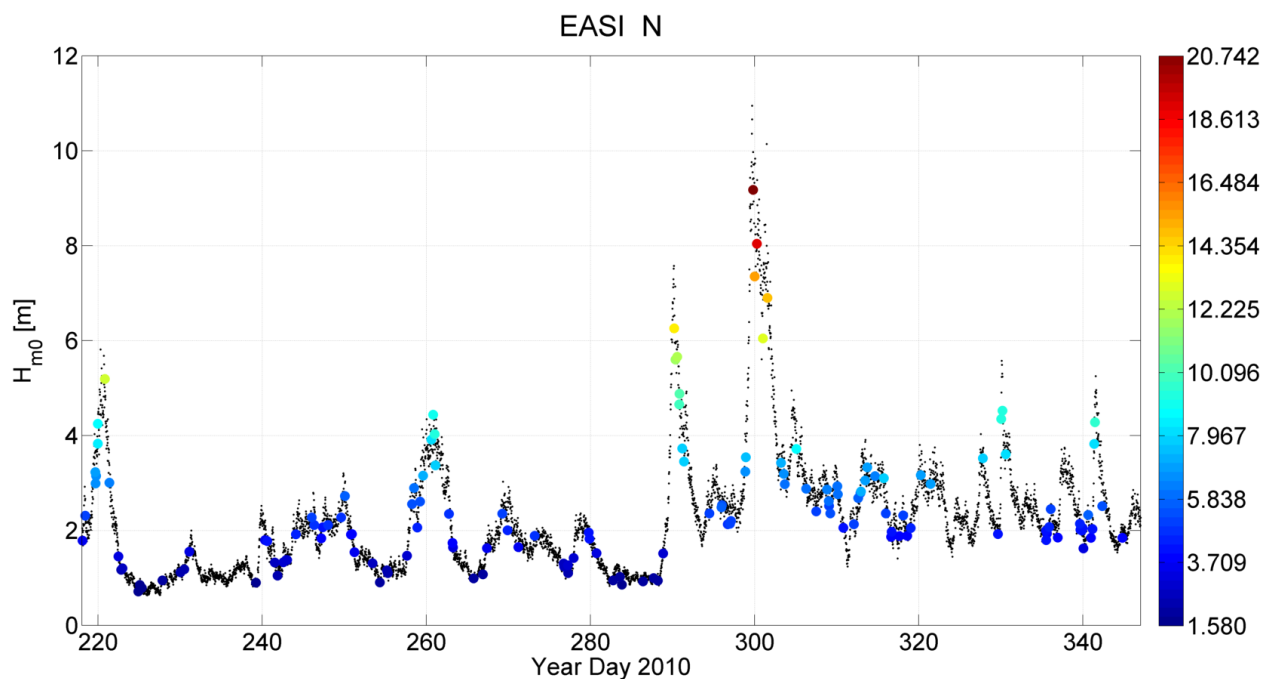
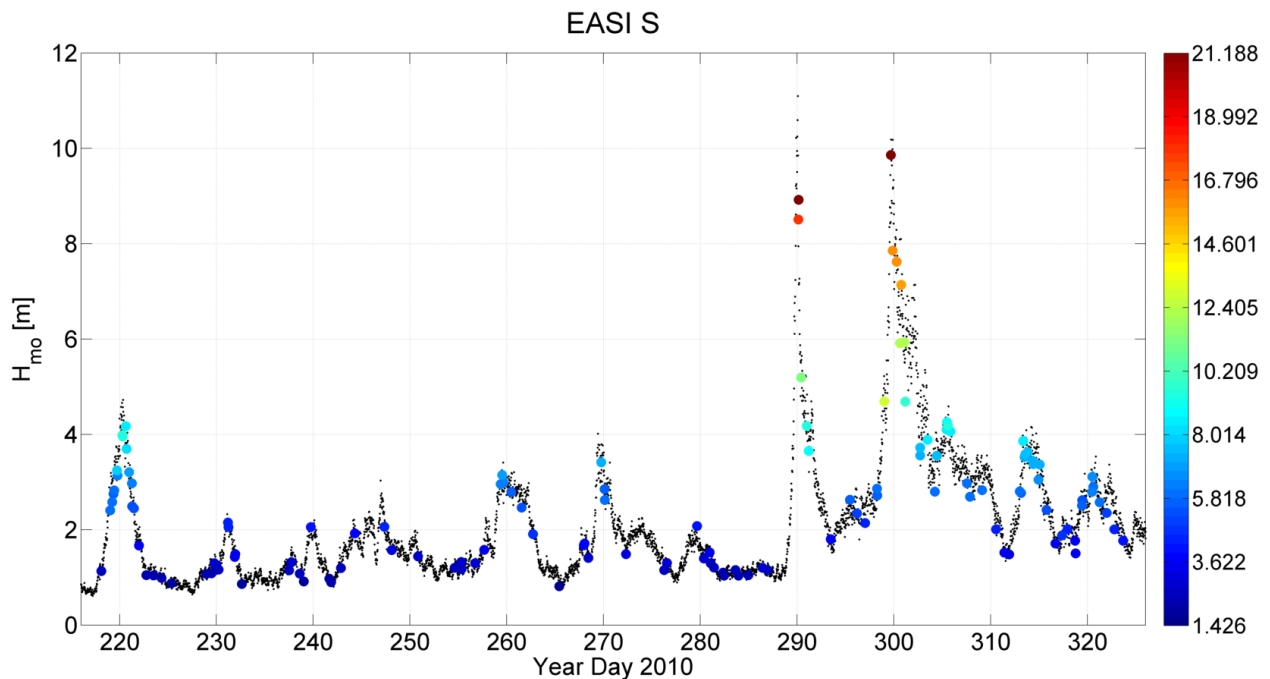


Figure 2) Time series of wave height over the ITOP experimental time period from EASI-N.  $H_{m0}$  is shown in black dots. The  $H_{max}$  are plotted in colored circles at each occurrence of a rogue wave. The color of the circle indicates the height [m] of  $H_{max}$ . The peak of the Dianmu, Fanapi, Malakas, Megi, and Chaba occurs in the  $H_{m0}$  data are year days ~220, ~260, ~270, ~292, and ~300, respectively.

### 1.3 TC WAVES

Many studies have explored the unique and interesting properties of waves which emanate from TCs. Of interest for this study is work which has focused on the asymmetry of wave field properties with respect to TC quadrant and the implications these asymmetries might hold for rogue wave development. It has been shown that the wave height under a TC is higher on the right side of the storm due to wind speed asymmetry, and, under certain conditions dynamic fetch (i.e. forward storm movement matching the group speed at the spectral peak). Other significant inhomogeneities of the TC forced wave field were largely uncovered by (Wright et al., 2001) with data from their scanning radar altimeter (SRA). This was followed up by further analysis of SRA data (Black et al., 2007; Holthuijsen, Powell, & Pietrzak, 2012) and numerical modeling (Moon et al., 2010). The conclusion is that far from the radius of maximum wind speed (RMW) swell typically radiates out from the right front quadrant and crosses with the local wind seas. Within a few RMW, the largest waves may be found in the right front quadrant where the swell is aligned with the wind, the left front contains crossed swell, and the rear of the storm may be characterized by opposing winds and waves. All of this may result in complicated bi-modal and sometimes tri-modal directional spectra.



**Figure 3) Time series of wave height over the ITOP experimental time period from EASI-S.  $H_{m0}$  is shown in black dots. The  $H_{max}$  are plotted in colored circles at each occurrence of a rogue wave. The color of the circle indicates the height [m] of  $H_{max}$ . The peak of the Dianmu, Fanapi, Malakas, Megi, and Chaba occurs in the  $H_{m0}$  data are year days ~220, ~260, ~270, ~290, and ~300, respectively.**

Mori, (2012) has considered rogue wave development within the quadrants of TCs. He used the SWAN wave model (Booij, Ris, & Holthuijsen, 1999) driven by a super gradient wind field to show spatial dependence of freak wave indexes within TCs including BFI. He found that the right-rear quadrant has the most non-linear wave height enhancement, and the left-rear quadrant is the most Gaussian but exhibits dangerous crossing seas. The findings were supported with

limited coastal observations. Further studies are needed to uncover more detailed information between TC quadrants and rogue waves.

## 2. METHODS

### 2.1 MOORINGS

Each EASI buoy, to be described further in section 2.2, was moored to the sea floor in a depth of ~5500 m. A single point inverse catenary style mooring system was employed with a scope (i.e. ratio of mooring length to water depth) of 1.26 to allow the buoy to follow the surface relatively unobstructed. The attachment point was a stainless steel yoke which was used to try and further isolate the buoy from mooring forces. The ~3100 kg mooring anchors (locomotive wheels) were located at 127.25 °E, 19.63 °N and 126.96 °E, 21.23 °N which amounts to a separation of about 180 km. These are referred to as the northern (-N) and southern (-S) moorings, respectively.



Further details of the mooring components may be found in Drennan et al. (submitted to JTECH). On September 17<sup>th</sup>, (Year Day (YD) 260), during typhoon Fanapi, the tether sheared apart and ASIS-N had to be recovered early.

Similarly, on October 22<sup>nd</sup> (YD 295), during typhoon Megi, the ASIS-S broke free of its tether requiring recovery.

The EASI buoys operated continuously for approximately 4 months, also described in full by Drennan et al. (submitted to JTECH), endured the relatively close passages of 4 major

tropical cyclones (TC), and received significant swell which radiated from a 5<sup>th</sup> TC. This unique dataset includes directional and non-directional wave information (Collins et al. submitted to JTECH).

### 2.2 BUOY DESIGN

EASI's ship-like hull is based on a NOMAD design which was originated in the 1940's as part of the U.S. Navy's offshore data collection program and has subsequently seen modern deployment by the National Oceanic and Atmospheric Administration's (NOAA) National Data Buoy Center (NDBC) and the Canadian Marine Environmental Data Service (MEDS). The configuration used in ITOP is completely unique from previous NOMAD deployments. Of interest to this study is the use of a motion pack with measured all 6 degrees of freedom (i.e. heave, pitch roll, surge, sway, yaw) which consisted of a triaxial linear accelerometer (Columbia Research Laboratories SA307-HPTX), three orthogonally mounted rate gyros (Systron Donner

model QRS110050 or SDG1000) and a compass (Precision Navigation TCM-2). The EASI buoys were treated as heave-pitch-roll surface following systems to obtain directional wave spectra. Crucially, Drennan et al. (submitted to JTECH) show that, for the energy containing region of the sea surface elevation spectrum, the EASI platform is a near perfect surface follower. For bulk parameters, EASI platforms were extensively compared and validated in Collins et al. (submitted to JTECH).

Let us mention here just a few caveats, pointed out in Dysthe, Krogstad, & Müller (2008), which should be kept in mind when dealing with buoy data (although the exact extent to which these generalizations may apply to the EASI platform is not known). Previous studies have shown that buoy data give statistics just under Gaussian wave theory. It has been proposed that this may be due to the buoys free horizontal movement which may allow for avoiding the highest waves (Krogstad & Barstow, 2000). Also, Dysthe, Krogstad, & Müller, (2008) stated that there is a belief that the wave profiles recorded by buoys are “less accurate”, but the statement was not substantiated.

Lastly, the physical size of the buoy (6 m x 3 m x 3 m) acts as a low pass filter. The buoy response falls off at wavelengths corresponding to ~0.45 Hz and shorter. Due to this size filtering, the statistics of short, small seas will not be accurately represented. This should not present a problem because the mean and standard deviation peak frequency over the experiment was  $0.125 \pm 0.024$  Hz (corresponding peak wavelength of  $124 \pm 50$  m). So, spectral parameters remain generally unaffected by the size filtering, particularly so for the highest sea states.

## 2.3 ANALYSIS

The nearly continuous dataset was split up into 30 minute blocks (5990 and 5101 blocks for EASI-N and -S, respectively). For each block, signals were recorded at 20 Hz, and average parameters and spectra were calculated from these signals. The time series of surface elevation,  $\eta$ , is defined by doubly integrating the tilt corrected vertical accelerometer,  $A_z$ :

$$\eta = \iint A_z dt dt = \iint (-a_1 \sin\theta + a_2 \cos\theta \sin\varphi + a_3 \cos\theta \cos\varphi - g) dt dt$$

Where  $a_1$ ,  $a_2$ ,  $a_3$ ,  $\theta$ ,  $\varphi$ , and  $g$  are surge, sway, heave, pitch, roll, and the gravitation constant, respectively. A rogue wave was defined as single apparent wave,  $H$ , (defined by zero-crossing analysis) the height (vertical distance from trough to crest) of which is at least double the significant wave height (SWH). Significant wave height may be defined statistically through observed wave height distribution as the mean of the 1/3 highest wave heights,  $H_{1/3}$ , or as an integral measure of the 1-D wave spectrum:

$$H_{m0} = 4\sqrt{m_0} = 4 \sqrt{\int_0^{\infty} S(f) df}$$

In this data set,  $H_{1/3}$  tends to be about 5% lower than  $H_{m0}$  [consistent with previous studies (Dysthe, Krogstad, & Müller, 2008)], so the total number of rogue waves was sensitive to the method of calculating SWH.  $H_{m0}$  is used to define SWH throughout the rest of this study.

$$H_{rogue} \geq 2H_{m0}$$

Down-crossing analysis gave slightly larger number of total rogue waves compared to up-crossing. In general, the ratio of the maximum individual wave height in a record to the  $H_{m0}$  is referred to as a freakish or abnormality index, but roguish index ( $RI$ ) is used instead accordance with the language established in this study.

$$RI = \frac{H_{\max}}{H_{m0}}$$

The parameter spaces, assuming uni-modal seas absent significant wind forcing, which completely define the nonlinear stability of the seas are metrics for steepness, bandwidth, and directional spread which are defined, respectively, by the following equations:

$$S_s = \frac{2\pi m_2 H_{m0}}{g m_0}$$

$$v = \sqrt{\frac{m_0 m_2}{m_1^2} - 1}$$

$$\sigma_p = \sqrt{2 \left( 1 - \sqrt{A_1^2(f_p) + B_1^2(f_p)} \right)}$$

Where the spectral and directional moments are integrals of the directional spectrum,  $E(f, \theta)$  subscript p refers to the values at the spectral peak:

$$m_n = \int_0^\infty f^n \left\{ \int_0^{2\pi} E(f, \theta) d\theta \right\} df$$

$$A + iB_n = \frac{1}{\pi} \int_0^{2\pi} e^{in\theta} E(f, \theta) d\theta$$

Inverse wave age ( $IWA$ ) is the ratio to the wind speed to the phase speed at the spectral peak,  $IWA = U_{10N}/c_p$ , and will be used to indicate the level of interaction between the wind and waves.

## 2.4 ERROR ANALYSIS

Calculating surface elevation from the accelerometer requires double integration. Integration is performed in frequency space by applying a Fourier transform (FFT) and then multiplying by a transfer function as follows:

$$\iint x(t) dt = \int_{-\infty}^{\infty} \frac{1}{(2\pi i f)^2} \hat{x}(f) df$$

A high pass filter (rectangular) is applied to deal with low frequency noise before returning the signal to a time series via IFFT. The convolution of this high pass filter introduces some spectral leakage. It is believed that this spectral leakage is the root of artificial amplitude enhancement at the beginning and at end of some records. More work on this issue is needed.

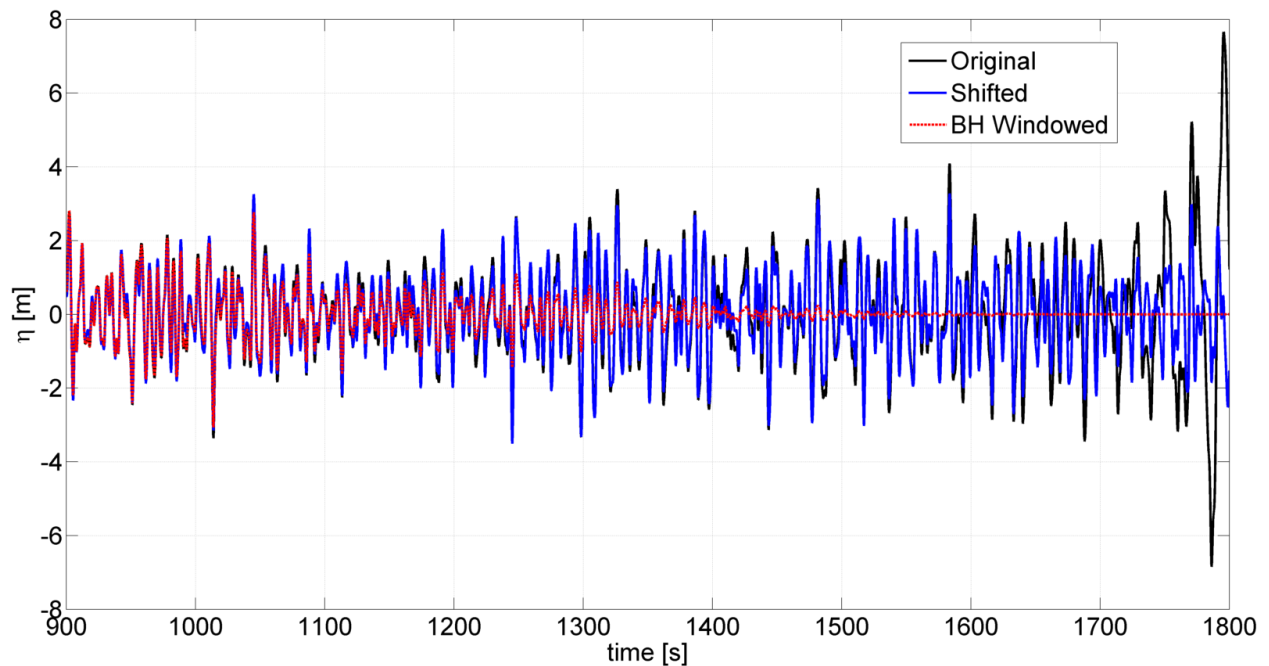


**Figure 4)** The second half of a thirty minute analysis block from EASI-S. The solid black line shows the surface elevation as a result of integrating the flatlined signals. The fixed data (beginning the analysis after the flatlines), referred to as shifted is shown in solid blue. The red dashed line shows the signal after the application is multiplied by a Blackman-Harris window as part of the spectral analysis.

In the EASI-S, the signal ramping was exacerbated by 60-90 s flatline in all recorded channels at the beginning of every 1/4<sup>th</sup> block. As a result of this artifact, many more rogue waves were found in EASI-S data during the preliminary analysis. Perhaps the simplest fix is chosen: removing the first 90s  $A_z$  of every 30 minute block from EASI-S. The loss of waves from good parts of the record (and those records without errors) is accepted for the tradeoff of reducing this error and maintaining simple analysis procedures. Fig (4) shows a comparison of the surface elevation,  $\eta$ , from the original  $A_z$  and one with the first 90s removed. It can be seen that the effect is localized to the first (not shown) and last few wavelengths. The plot also shows the Blackman-Harris (BH) window which is used before applying a FFT for spectral analysis. The BH window removes the artificial part of the record; therefore these errors were not factored into calculation of spectral parameters (i.e.  $H_{m0}$ ).

### 3. RESULTS

#### 3.1 STORMS

2010 was a tropically active year for the Pacific basin with 14 named storms. The tracks of 4 of these storms were relative close to the mooring sites. In chronological order, the effects of the following storms can be found in the time series of  $H_{m0}$  [e.g. Figs (2) and (3)]: severe tropical storm Dianmu around 8 August 2010 (YD ~220), typhoon Fanapi around 18 September (YD ~260), Typhoon Malakas around 28 September 2010 (YD ~270), Super Typhoon Megi on 17 October 2010 (YD ~290), and Typhoon Chaba around 17 October 2010 (YD ~300); from here

on referred to by name only. Best-track estimates and estimated maximum wind speeds (from Joint Typhoon Warning Center) can be seen in Fig (1).

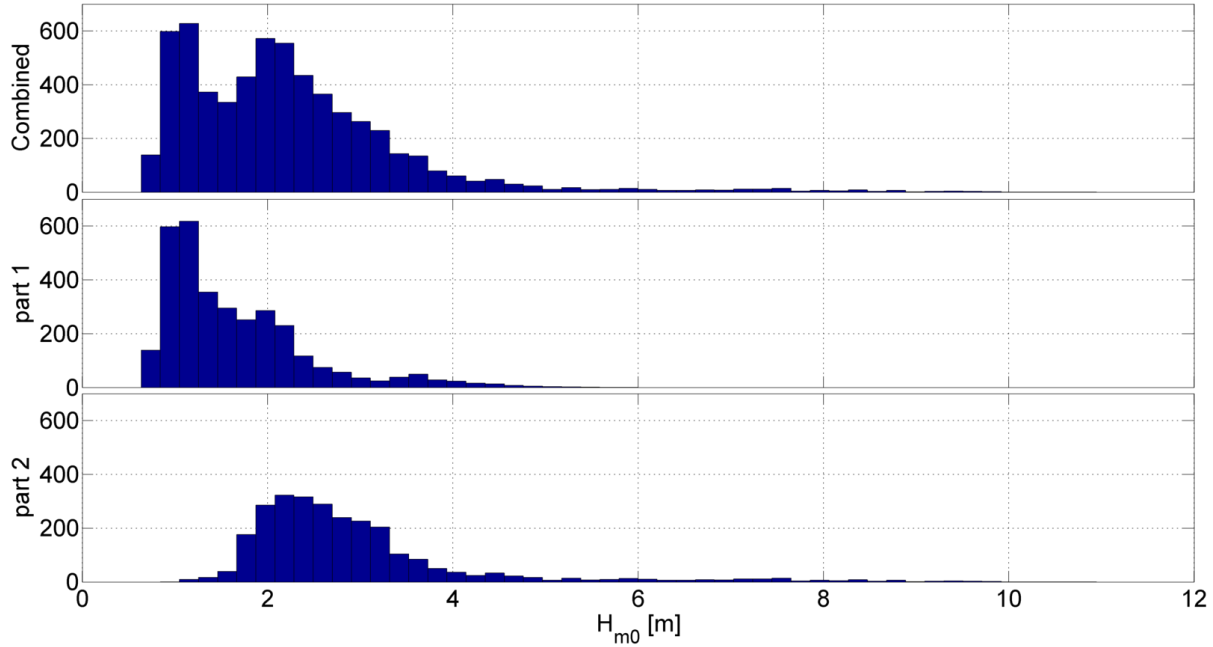


Figure 5) The wave height distributions from EASI-N (from top panel to bottom panel) of the entire ITOP experimental period (i.e. two parts combined together), the period referred to as part 1 separated, and the period referred to as part 2 separated.

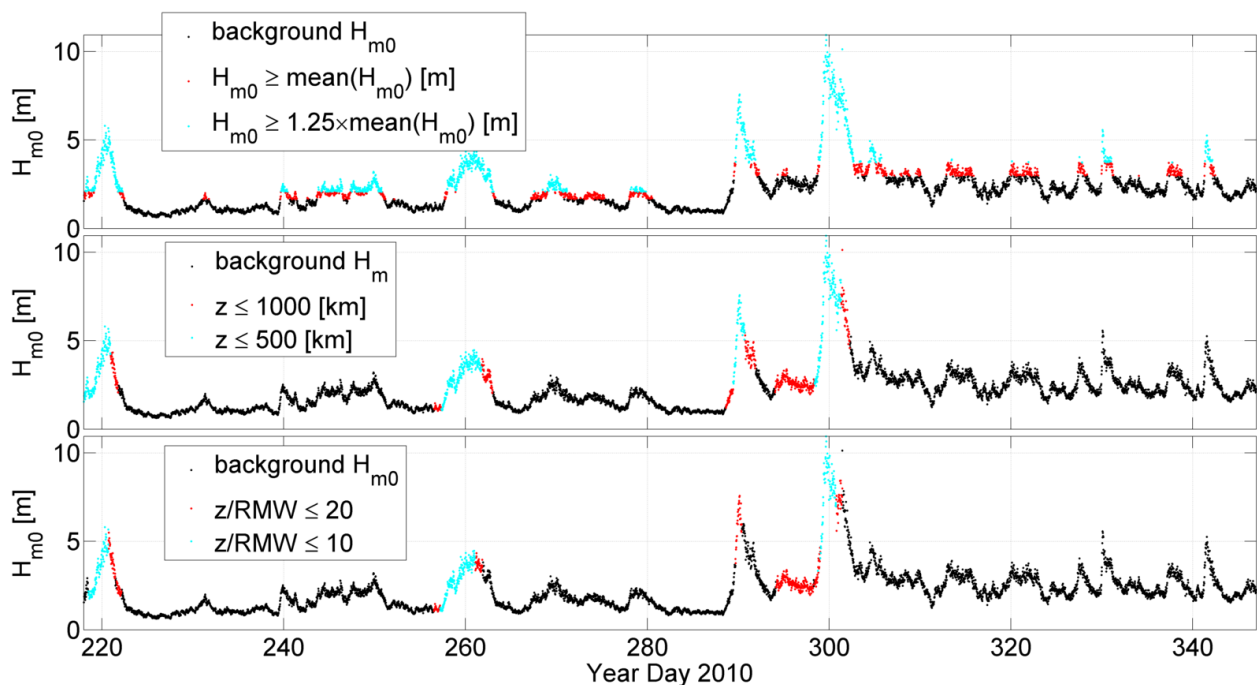
Here the possible influence of Tropical Cyclones on the probability of observing a rogue wave is explored. To define storms in the time series a threshold method was used which was defined in context of the mean wave height. The dataset shows a sort of seasonal variability of the distribution of wave height which transitions at the beginning of Megi.

Table 1) The length in YDs, mean  $H_{m0}$ ,  $\max(H_{m0})$ , total number of rogue waves, and the number of rogue days are given for part 1, part 2, and the combined parts for EASI-N and -S. Rogue days are defined as days with at least 2 (3) rogue waves occurring that day.

Period/Characteristic	Length [YD]	Mean $H_{m0}$ [m]	Max $H_{m0}$ [m]	Rogues	Rogue Days >2 (>3)
North Combined	129	2.3	10.9	158	45 (20)
North part 1	70	1.7	5.8	80	23 (8)
North part 2	59	3.0	10.9	78	22 (12)
South Combined	110	2.3	11.2	147	37 (15)
South part 1	73	1.7	4.8	83	19 (7)
South part 2	37	2.9	11.2	64	18 (8)

Therefore the data was split before and after the 17<sup>th</sup> (18<sup>th</sup>) October 2010 for EASI-N (-S) which is referred to as “part 1” and “part 2” of the times series, respectively. As an example, the distributions of the significant wave height for part 1, part 2, and the combination over the whole experiment are shown in Fig (5) for the EASI-N. Because the wave height distribution is remarkably different during the part 1 and part 2 of the experiment, statistical characteristics [see Table (1)] were defined separately for both these two parts and for EASI-N and -S.

It is of interest to capture the high wave periods in the time series in which TC winds are the dominate generator of the waves. It is possible to define the effect of a storm in time by several different metrics or perspectives. One may choose local metrics of wave height, wind speed, and/or pressure, but this will not directly discriminate for TCs. Or one may chose TC dependent metrics such as spatial distance (defined either by km or km normalized by RMW) between the measurement and the TC or TC strength (i.e. maximum wind speed, central pressure). Below 3 different metrics were plotted, and two cases for each metric. One case plotted in cyan is always a subset of the other case plotted in red so cyan cases represent more selective criteria. From top to bottom the metrics are based on local  $H_{m0}$  threshold, absolute geographic distance to storm center, and distance to storm center divided by RMW.



**Figure 6) Storm selection criteria based on three different metrics as applied to EASI-N. From top to bottom the metrics are  $H_{m0}$ , distance to center of the storm, and the distance to the storm center normalized by RWS.**

The wave height threshold [Fig (6) top panel] works well in capturing the entirety of the high wave events due to the TC’s, but the metric cannot discriminate between TC and non-TC high wave cases. The metric defined by absolute geographic distance [Fig (6) center panel] performs well with the less selective option (red dots), but this metric ignores the decaying wave field after the storm has left the region. Note in Fig (6) in the center and bottom panels Malakas no longer meets the criteria for storm analysis due to distance. This is undesirable because the decaying wave fields from storms which passed and the waves from Malakas are obviously still TC

generated waves. Consequently, these should still be classified “storm” periods even if the storm effects are no longer direct and local. The metric defined by geographic distance normalized by RMW [Fig (6) bottom panel] looks similar to the non-normalized option (though a bit more selective) except for the case of Megi which has been nearly cut out of the analysis for EASI-N due to an unusually small RMW.

In the end, a somewhat hybrid method is utilized. First, the storm periods are defined by  $H_{m0}$  threshold (EASI-N) [i.e. as in the top panel in Fig (6)], and then specific knowledge of the storms was used to disregard non-TC periods. So, technically the storms starts when  $H_{m0}$  is above average and ends when there are at least three consecutive points below average. This way the waves generated by TCs are isolated but include both the building and decaying wave fields. The results of this analysis is shown in Table (2).

**Table 2) Data was taken from both EASI-N and -S to give the total number of rogue waves per TC. Then these are combined to make up the total TC and non-TC periods. This is done again excluding Malakas from the TC analysis and marked by the asterisk (\*). The total combined datasets is shown in the last row for reference. The last column is Occurrence Probability (OP) which is simply the number of observed rogues divided by the number of waves in the analysis.**

Storm	# of Rogues	# of Waves	OP [ $10^{-4}$ ]
Dianmu	28	106814	2.62
Fanapi	18	137964	1.30
Malakas	7	126486	0.55
Megi	13	60998	2.13
Chaba	31	153573	2.02
Combined TC	97	585826	1.66
non-TC	208	2752171	0.76
Combined TC*	90	459349	1.96
non-TC*	215	2878657	0.75
<b>Total</b>	<b>305</b>	<b>3338006</b>	<b>0.91</b>

#### 4. DISCUSSION

Figs (2) and (3) present  $H_{m0}$  and  $H$  for the occurrence of the rogue waves. Note that this obscures a few rogue waves that occur during the same 30 minute block (6 and 10 in EASI-N and -S). Though included in the analysis in Table (2), these double rogue records would also be masked by more standard data analysis in which only  $H_{max}$  and  $H_{m0}$  are recorded: an advantage of recording the full time series. A total of 305 rogue waves were recorded, and 9 of these qualified as extreme rogues ( $\geq 15$  m). The highest individual wave height recorded for EASI-N and -S was 20.7 m and 21.2 m, respectively. The highest roguish index recorded was 2.7.

The most significant result of this preliminary analysis is that time periods forced by TCs show an unambiguous increase in the number of observed rogue waves except for Malakas. Recall that the waves measured from Malakas were created at a large distance to the storm. By the time these waves reached the moorings they had dispersed and organized into swell. Therefore, the wave parameters from Malakas were more similar to a non-TC time. Table (2) shows the same

analysis for TC and non-TC periods including and excluding Malakas. This result is slightly more striking without including Malakas in the TC analysis.

It is difficult to comment on the exact cause of the increased number of rogue waves during TCs. When the TC seas are building, the seas are young and hence highly forced seas. Although, increased steepness, decreased directional spread, and decreased bandwidth lead to unstable seas, it is known that these indices do not directly correlate with *RI* (Waseda, Kinoshita, & Tamura, 2009). Table (3) shows spectral parameters of  $S_S$ ,  $\nu$ ,  $\sigma_p$ , and *IWA*.

Referring to Table (3), the differences between the periods marked by TCs and non-TC periods are most substantial for the parameters of  $S_S$  and *IWA*. The difference in bandwidth is not significant, and the directional spread is slightly increased for the TC periods which is opposite of what one would expect for unstable seas. This suggests that increased steepness may be the most important feature of TC seas in the context of observing a rogue wave. As for *IWA*, rogue wave suppression or excitation through interaction with wind is still an open question [e.g. see Babanin, (2013)].

**Table 3) Per buoy spectral parameters and IWA which are indices of unstable seas. The asterisk (\*) denotes that the dataset excludes Malakas. The coptic small letter dei (†) means that the dataset for calculating this parameter was limited due to sensor failure.**

Buoy	$S_S$	$\sigma_p$ [°]	$\nu$ [Hz]	<i>IWA</i>
EASI-N TC*	0.052	34.84	0.72	0.80
EASI-N non-TC*	0.036	37.41	0.70	0.59
EASI-S TC*	0.050	34.89	0.73	0.74 <sup>†</sup>
EASI-S non-TC*	0.032	39.67	0.71	0.45 <sup>†</sup>

## 5. FUTURE WORK AND CONCLUSION

It is hypothesized that building and decaying seas will have different spectral characteristics and IWAs. It will be interesting to further analyze rogue wave occurrences by splitting up the building and decaying seas. Another question not addressed regards the differences between TC seas and other stormy seas. Is there any reason to suspect that other types of storms would not show increased rogue wave occurrences? Although significant differences between TC and non-TC periods were found, is this unique to TCs or may these properties be found during any high wind event? TC structure is unique in terms of very limited fetch due to circular wind pattern. Within this limited fetch, the winds may be very strong and transfer a great deal of momentum into the waves especially in dynamic fetch situations. Does the spectrum of waves created in these unique TC situations differ significantly from a typical low pressure system which would be more broad (larger fetch) but possess less powerful winds?

This work will be followed up by analyses which attempt to verify some other theoretical and numerical studies. Following the results of Janssen (2003), Mori & Janssen (2006), and Waseda, Kinoshita, & Tamura (2009), kurtosis (the 4<sup>th</sup> moment of surface elevation) has been shown to be correlated with *RI* and may be a key indicator of dangerous seas. They have proposed a probabilistic forecasting of rogue waves which is directly related to kurtosis calculated from the spectrum (narrow band width assumption). The dataset may be used to support these findings

since kurtosis may be calculated from the time series of surface elevation directly and compared that with the spectrally derived kurtosis and  $RI$ .

The analysis was focused in the time domain, but, as mentioned in section 1.3, there is interest in understanding the spatial distribution of wave parameters in TCs and what this implies for the probability and occurrence of rogue waves. Fig (7) shows the spatial distribution of the ITOP data in a composite, TC centered plot. It is planned to further analyze the data to see if spectral parameters dependent on quadrant and distance from RMW in way consistent with previous studies. It needs to be noted that this dataset, although relatively rich and unique, is hardly exhaustive in terms of quadrant sampling, storm strength, RMW, storm translation speed, directional change of the storm translation, and other storm parameters.

Other future work will examine the kinematic nature of the extreme rogues. What is the structure of these extreme rogues (i.e. do they exhibit strong vertical or horizontal asymmetry, is it within a group of larger waves), and are they somehow different from smaller scale rogue waves?

In conclusion, a comprehensive, quality controlled, deep-water dataset for studying rogue waves and waves generated by TCs is presented. Preliminary analysis has found increased observations of rogue waves in the vicinity of TCs. This may be related to the increased wave steepness which enhances modulation instability during these storms. The potential for future efforts using this dataset is great, and it is hoped that later findings might be applied to make sea travel and operations safer.

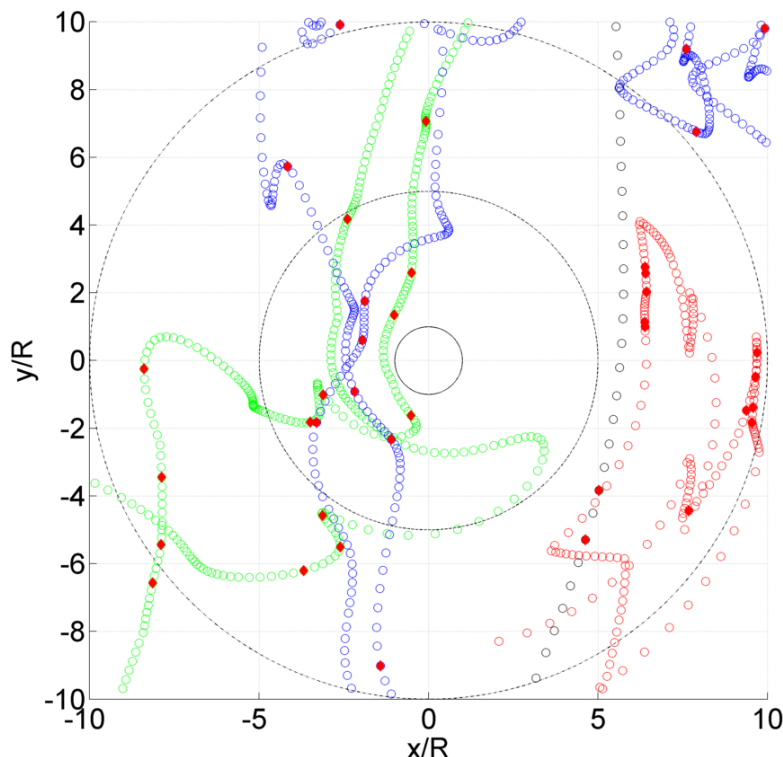


**Figure 7) Composite map of all TCs encountered during ITOP. This is a storm centered view with the storm translation direction in the positive y (up page) direction. The geographic distance in the x and y direction is normalized by the RMW (here simply R). The data during Dianmu, Fanapi, Megi, and Chaba are shown in red, green, black, and blue open circles, respectively. The red diamonds represent blocks in which rogue waves were observed.**

## ACKNOWLEDGEMENTS

This work benefited through many conversations with Dr. Takuji Waseda (University of Tokyo) who was very generous with his time and a hospitable host during the summer of 2013. Dr. Björn Lund (RSMAS) read and improved this manuscript. My work and my attendance at this conference is supported by advisor Dr. Hans C. Graber (RSMAS). I also thank RSMAS professors Dr. C. Linwood Vincent, Dr. William M. Drennan, and Dr. Brian K. Haus for useful conversation regarding this and other related work. ITOP funding was provided by the U.S. Office of Naval Research grant #N00014-09-0392. Part of this work was done at the University of Tokyo under a NFS EAPSI fellowship which is a joint partnership with the JSPS summer program.

## REFERENCES

- Babanin, A. (2013). A physics-based approach to wave statistics and probability. *Proceedings of the ASME 2013 32nd International Conference on Ocean, Offshore and Arctic Engineering*, Nantes, France. pp. 1-12.
- Black, P. G., D'Asaro, E. A., Drennan, W. M., French, J. R., Niiller, P. P., Sanford, T. B., et al. (2007). Air-sea exchange in hurricanes. *Bull. Amer. Meteo. Soc.*, 88(3), 357-374.
- Booij, N., Ris, R. C., & Holthuijsen, L. H. (1999). *A third-generation wave model for coastal regions. I- model description and validation* Journal of Geophysical research.
- Collins III, C.O.; Lund, B.; Ramos, R.J., Drennan, W.M.; Graber, H.C., Wave Parameter Inter-Comparison and Platform Evaluation during the ITOP (2010) Experiment. (Submitted to JTECH).
- Drennan, W.M.; Graber, H.C.; Collins III, C.O.; Williams, N.J.; Ramos, R.J.; Potter, H.; Herrera, A., EASI: An air-sea interaction buoy for high winds. (Submitted to JTECH).
- Dysthe, K., Krogstad, H. E., & Müller, P. (2008). Oceanic rogue waves. *Annual Review of Fluid Mechanics*, 40(1), 287 - 310.
- Graber, H. C., Terray, E. A., Donelan, M. A., Drennan, W. M., van Leer, J. C., & Peters, D. B. (2000). ASIS—A new Air–Sea interaction spar buoy: Design and performance at sea. *Journal of Atmospheric and Oceanic Technology*, 17(5), 708-720.
- Holthuijsen, L. H., Powell, M. D., & Pietrzak, J. D. (2012). Wind and waves in extreme hurricanes. *J.Geophys.Res.*, 117, 09003.
- Janssen, P. A. (2003). Nonlinear four-wave interactions and freak waves. *Journal of Physical Oceanography*, 33(4), 863-884.
- Krogstad, H. E., & Barstow, S. F. (2000). Unified approach to extreme value analysis of ocean waves. *PROC INT OFFSHORE POLAR ENG CONF*, , 3. pp. 103-108.
- Moon, I. J., Ginis, I., Hara, T., Tolman, H. L., Wright, C. W., & Walsh, E. J. (2010). *Numerical simulation of sea surface directional wave spectra under hurricane wind forcing*
- Mori, N. (2012). Freak waves under typhoon conditions. *J.Geophys.Res.*, 117, C00J07.
- Mori, N., & Janssen, P. A. E. M. (2006). On kurtosis and occurrence probability of freak waves. *Journal of Physical Oceanography*, 36(7), 1471-1483.

Tamura, H., Waseda, T., & Miyazawa, Y. (2009). Freakish sea state and swell-windsea coupling: Numerical study of the suwa-maru incident. *Geophysical Research Letters*, 36(1), L01607.

Waseda, T., Hallerstig, M., Ozaki, K., & Tomita, H. (2011). Enhanced freak wave occurrence with narrow directional spectrum in the north sea. *Geophysical Research Letters*, 38(13)

Waseda, T. (1999). Experimental study of the stability of deep-water wave trains including wind effects. *Journal of Fluid Mechanics*, 401(1), 55.

Waseda, T., Kinoshita, T., & Tamura, H. (2009). Evolution of a random directional wave and freak wave occurrence. *Journal of Physical Oceanography*, 39(3), 621-631,634-639.

Waseda, T., Tamura, H., & Kinoshita, T. (2012). Freakish sea index and sea states during ship accidents. *Journal of Marine Science and Technology*, 17(3), 305-314.

Wright, C. W., Walsh, E. J., Vandemark, D. C., Krabill, W. B., Garcia, A. W., Houston, S. H., et al. (2001). Hurricane directional wave spectrum spatial variation in the open ocean. *Journal of Physical Oceanography*, 31(8), 2472-2488.